

# Polymer Nanocomposites through Controlled Self-Assembly of Cubic Silsesquioxane Scaffolds

Lei Zheng,<sup>†</sup> Sheng Hong,<sup>‡</sup> Grégoire Cardoen, Engin Burgaz, Samuel P. Gido, and E. Bryan Coughlin\*

Polymer Science and Engineering Department, University of Massachusetts, Amherst, Massachusetts 01003

Received July 15, 2004; Revised Manuscript Received August 26, 2004

**ABSTRACT:** A novel bottom-up approach to obtain polymer nanocomposites using cubic silsesquioxanes (POSS) nanoparticles as building blocks is reported. The design is based on associative interaction between particles to form ordered nanostructure and limited crystal growth to render anisotropic shapes. Specifically, the affinity between POSS units causes these particles to aggregate and closely pack into a crystalline lattice. The organic polymer, covalently connected to each POSS unit, limits the crystallization into a two-dimensional lattice as demonstrated in random copolymers of polybutadiene and cubic silsesquioxanes. The copolymers were synthesized by ring-opening metathesis copolymerization of cyclooctadiene and POSS bearing a polymerizable norbornene group. The polymers were characterized using NMR, DSC, TEM, WAXD, and SAXS. The data from TEM and X-ray diffraction clearly show the formation of two-dimensional lamellar-like nanostructures of assembled cubic silsesquioxanes.

## Introduction

**Background.** The formation of ordered structures at the nanometer length scale requires strategies that are able to harness the fundamental forces of self-assembly to direct the generation of higher ordered motifs from the basic building block constituents.<sup>1–3</sup> Utilization of noncovalent interactions, both intra- and intermolecular, remains one of the principal scaffolds upon which nanoscale aggregates are constructed. For polymers, success has been achieved using organic block copolymers to generate a range of differing nanometer length scale morphologies in the solid state. The generation of these structures is driven by reducing surface energy between chemically linked, yet incompatible, blocks.<sup>4,5</sup> A limitation remains, however, in that long annealing times are needed to approach thermodynamically favorable structures in block copolymer morphologies. Comparable nanoscale morphological structures have been obtained for inorganic–polymeric structures using sol–gel preparative methods utilizing amphiphilic surfactants as templates.<sup>6–8</sup> There is, however, the associated problem of maintaining the desired structure upon removal of the surfactants. A considerable challenge remains how to construct robust nanostructured materials directly using suitable building blocks from the bottom-up. Controlling associative interactions of scaffold components is certainly an attractive route. However, implicit in this approach is developing an understanding of the interplay of noncovalent interactions to the extent that there is then the ability to manipulate polymeric structures. Ultimately, with a tailored primary chemical sequence, desired ordering of the secondary structure at length scales considerably longer than those of the individual polymer chain could be achieved.

<sup>†</sup> Current address: The Goodyear Tire and Rubber Company, 1485 E Archwood Av, Akron, OH 44306.

<sup>‡</sup> Current address: Atofina Chemicals Inc., 900 First Ave., King of Prussia, PA 19406.

\* To whom correspondence should be addressed. E-mail: coughlin@mail.pse.umass.edu.

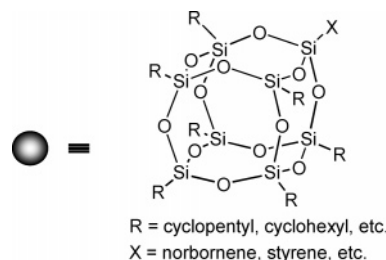


**Figure 1.** Structure of cubic silsesquioxanes (POSS). Cubic silsesquioxane is a well-defined molecule having an inorganic core comprised of  $\text{Si}_8\text{O}_{12}$  surrounded by eight tunable substitution groups. Each unit can be treated as a sphere represented by a gray ball in all the following figures.

Polyhedral oligomeric silsesquioxanes (POSS) are a family of molecularly precise nearly isotropic molecules with diameters ranging between 1 and 3 nm, depending on the number of silicon atoms in the central cage and the peripheral substitution groups surrounding this core.<sup>9</sup> A cubic  $\text{T}_8$  silsesquioxane unit has an inorganic cubic core comprised of  $\text{Si}_8\text{O}_{12}$  surrounded by eight tunable substitution groups, i.e., cycloaliphatic groups (Figure 1). It has an approximate spherical diameter of 1.5 nm when R is a cyclopentyl group. POSS has been recognized as well-defined building blocks for nanostructured materials.<sup>10–13</sup> Efficient synthetic methods have also been developed whereby one, or more, of the corner groups are substituted by a functional group X capable of undergoing polymerization. This has provided the possibility to incorporate inorganic POSS cages into organic polymer chains.<sup>9–11,13–33</sup> The cubic silsesquioxane unit can be viewed as a nanoparticle for both its size and filler function or a well-defined macromonomer for its ability to undergo polymerization. In this paper, we also demonstrate its use as a scaffold to generate lateral ordering as a consequence of polymer–POSS interactions.

**Design Rationale.** A body of work has shown that octaalkyl-substituted cubic silsesquioxane nanoparticles  $\text{R}_8\text{Si}_8\text{O}_{12}$  form hexagonal (or equivalently rhombohedral) crystal structures.<sup>34–39</sup> On the basis of X-ray studies

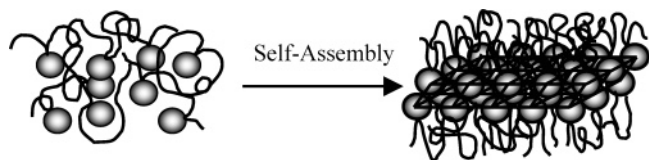


**Figure 2.** Synthesis of polymer nanocomposites through controlled self-assembly of cubic silsesquioxane (POSS) nanoparticles. POSS preferentially aggregate and crystallize into an ordered lattice within the polymer matrix. The covalently bonded polymer chains serve as the source of confinement to limit POSS growth in a two-dimensional lattice.

from Larsson<sup>35</sup> and recent work from this laboratory,<sup>40</sup> each cubic silsesquioxane unit can be regarded as being nearly spherical. The three-dimensional crystal structure of POSS can be viewed by arranging each POSS sphere in a plane on a hexagonal array and stacking these planes in ABCA sequence. When POSS spheres are attached along polymer chains, the crystal packing of the cubic silsesquioxane units is constrained by their covalent attachment to the polymer chain. As a result, a bilayer or lamella-like structure is formed where POSS spheres are packed hexagonally within planes and two planes are stacked together. In other words, the covalently connected chains serve as the source of crystallization confinement, preventing the development of spherical packing in three dimensions, and therefore results in a two-dimensional raftlike structure. A schematic drawing is shown in Figure 2. The specific interactions between particles originate from intermolecular van der Waals forces, resulting in the stable construction of a nanolayered structure. In our previous study of polyethylene–POSS copolymers, X-ray diffraction data supported this proposed structure.<sup>38,41</sup> However, the competing cocrystallization of polyethylene frustrates the POSS assembly, and no large-scale POSS nanostructures were observed in real-space imaging techniques. In this study, a low glass transition temperature amorphous polymer, polybutadiene, was selected as the backbone polymers, thus providing a rubbery liquidlike matrix to allow the pendant POSS units to assemble in the absence of competing polymer crystallization.

## Experimental Section

**Materials.** Cyclopentyl-POSS-norbornene macromonomer 1-[2-(5-norbornen-2-yl)ethyl]-3,5,7,9,11,13,15-heptacyclopentylpentacyclo[9.5.1.1.3.9.1.5.15]1,7,13]octasiloxane (POSS-norbornene, **1**) was provided by Hybrid Plastics. The catalyst  $\text{RuCl}_2(\text{=CHPh})(\text{PCy}_3)_2$  was purchased from Strem Chemical. Other reagents were obtained from Aldrich. Cyclooctadiene and methylene chloride were vacuum-transferred from  $\text{CaH}_2$  prior to use.

**Polymerization Procedures for Polybutadiene-POSS Copolymers.** 9.74 mg (12  $\mu\text{mol}$ ) of  $\text{RuCl}_2(\text{=CHPh})(\text{PCy}_3)_2$  was dissolved in 1 mL of  $\text{CH}_2\text{Cl}_2$  and added to a solution of 0.65 g of cyclooctadiene (6 mmol, 500 equiv) and 0.072 g of POSS-norbornene **1** (0.070 mmol, 10 wt %) in 4 mL of  $\text{CH}_2\text{Cl}_2$  in the glovebox. The reaction mixture was stirred for 24 h under nitrogen at room temperature. The solutions remained homogeneous throughout the entire reaction. The reaction was stopped by injection of 1 mL of  $\text{CH}_2\text{Cl}_2$  with a trace amount of ethyl vinyl ether and 2,6-di-*tert*-butyl-4-methylphenol. The copolymers were precipitated in 100 mL of methanol, recovered by decanting the solvent, and dried overnight under vacuum at room temperature. The polymerizations were repeated using varying amounts of **1**, 0, 10, 20, 30, 40, and 50 wt %, to prepare a range of copolymers. The isolated yields were generally above 80%.

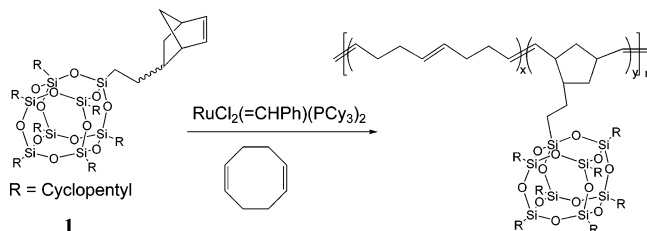


**Figure 3.** Synthesis of PBD–POSS copolymers. The copolymers were synthesized by ring-opening metathesis copolymerization of 1,5-cyclooctadiene and POSS bearing a polymerizable norbornene group.

**Polymer Characterization.**  $^1\text{H}$  spectra were obtained in chloroform-*d* at 300 MHz using a Bruker DPX-300 FT-NMR spectrometer.  $^{13}\text{C}$  NMR spectra were recorded in chloroform-*d* with a Bruker DPX-300 FT-NMR spectrometer operating at 75 MHz. High-temperature NMR were recorded in tetrachloroethane-*d*<sub>2</sub> with a Bruker AMX-500 FT NMR spectrometer operating at 125 MHz. Gel permeation chromatography was performed using a Polymer Lab LC1120 HPLC pump equipped with a Waters differential refractometer detector. The mobile phase was THF with a flow rate of 1 mL/min. Separations were performed using  $10^5$ ,  $10^4$ , and  $10^3$  Å Polymer Lab columns. Molecular weights were calibrated versus narrow molecular weight polystyrene standards.

**DSC.** Differential scanning calorimetry was performed under a continuous nitrogen purge on a Mettler-Toledo DSC 822<sup>e</sup>. Octane (Aldrich, 99%+), pentane (Aldrich, 99%+), deionized water, indium, and zinc were used to perform the calibration. Samples having a mass between 2.5 and 11 mg were used. Data were gathered using a scan rate of 10 °C/min on the first scan.

**TEM.** Specimens for TEM, WAXD, and SAXS were cast from 5 wt % toluene or methylene chloride solutions overnight in the hood. Bulk film samples for electron microscopy were microtomed in a Leica Ultracut cryoultramicrotome. Sections approximately 50–100 nm thick were cut with a Diatome diamond knife at a sample temperature of  $-110$  °C, a knife temperature of  $-100$  °C, and a cryogenic sample chamber of  $-120$  °C. The only exception was the sample PBD-POSS-1 because of the difficulty in handling a viscous liquid at room temperature. This sample was deposited onto the TEM grids directly from a dilute methylene chloride solution ( $\sim 0.1$  wt %), and the solvent was evaporated within minutes. TEM studies were performed using a JEOL 100 CX transmission electron microscope operated at 100 kV.

**WAXD.** Wide-angle X-ray diffraction was carried out on a Siemens D500 instrument in normal/transmission mode (0.3 incident slit beam divergence) with Ni-filtered  $\text{Cu K}\alpha$  radiation (1.54 Å wavelength). Data were obtained with the incident beam normal to the plane of the film.

**SAXS.** Small-angle X-ray scattering was performed using Ni-filtered  $\text{Cu K}\alpha$  radiation (1.54 Å wavelength) from a Rigaku rotating anode (operated at 40 kV, 200 mA). The X-ray was collimated by a set of three pinholes. A CCD detector (Siemens Hi-Star), located at a camera length of 875.2 mm, was used to record scattering patterns.

## Results and Discussion

**Polymerization.** To demonstrate the concept of controlled self-assembly of cubic silsesquioxane scaffolds, a series of random copolymers comprising polybutadiene (PBD) and POSS spheres were designed. The copolymers were synthesized utilizing ring-opening metathesis copolymerization (ROMP) of 1,5-cyclooctadiene and cubic silsesquioxane bearing a polymerizable norbornene group **1** using the catalyst  $\text{RuCl}_2(\text{=CHPh})(\text{PCy}_3)_2$  (Figure 3).<sup>42</sup> ROMP of cyclooctadiene provides exclusively 1,4-polybutadiene as the polymer backbone. The mole ratio of cyclooctadiene to catalyst was fixed at 500:1 to yield moderately high molecular weight

Table 1. Summary of Molecular Weight Data of PBD-POSS Copolymers

entry	sample	POSS (wt %) in feed	POSS in copolymer <sup>a</sup>		$M_w^b$ (kg/mol)	PDI <sup>b</sup>	trans/cis <sup>c</sup>
			wt %	mol %			
1	PBD	0	0	0	68	1.7	61:39
2	PBD-POSS-1	10	12	1.4	67	1.7	56:44
3	PBD-POSS-2	20	23	3.0	71	1.8	53:47
4	PBD-POSS-3	30	33	5.0	74	1.8	57:43
5	PBD-POSS-4	40	43	7.5	79	1.9	55:45
6	PBD-POSS-5	50	53	10.8	88	2.0	51:49

<sup>a</sup> As determined by <sup>1</sup>H NMR in CDCl<sub>3</sub>. <sup>b</sup> Weight-average molecular weight as determined by GPC in THF, vs narrow molecular weight polystyrene standards. <sup>c</sup> Trans/cis ratio of backbone unsaturations as determined by <sup>13</sup>C NMR of olefin region in CDCl<sub>3</sub>.

polybutadiene. Increasing concentrations of POSS were used in the reaction feeds to afford a series of random copolymers. The molecular weight characterization data of the PBD-POSS copolymers are listed in Table 1. All of these copolymers have  $M_w$  values between 67 and 88 kg/mol, and the corresponding polydispersities are in the range 1.7–2.0.

Using <sup>1</sup>H NMR to determine the level of incorporation of POSS macromonomer in the copolymers revealed a steady increase as the amount of POSS in the feed was increased. Samples with different incorporation of POSS (12–53 wt %) were obtained simply by changing the feeding ratio between cyclooctadiene and POSS. The physical appearance of the isolated products changes drastically from viscous liquid at 0 wt % POSS to elastomeric materials with 23 wt % or greater POSS loadings. The <sup>1</sup>H NMR also reveals no residual POSS-norbornene macromonomer in the copolymers. However, the conversion of cyclooctadiene to polybutadiene was not complete under the relatively dilute solution polymerization conditions (0.65 g of cyclooctadiene in 5 mL of CH<sub>2</sub>Cl<sub>2</sub>). The thermodynamic equilibrium among copolymer, cyclic oligomer, and residual monomer resulted in the maximum conversion being roughly 80%. Dilute solution polymerization was used instead of neat bulk polymerization, or concentrated conditions, simply due to the limited solubility of POSS macromonomer (~100 mg/mL). The wt % and mol % of POSS in the copolymers obtained from <sup>1</sup>H NMR agree with the feed ratio if the overall conversion of cyclooctadiene is considered. We believe that the backbone sequences of these copolymers are random, not blocky, on the basis of the efficient cross-metathesis mechanism between polymer chains as described previously.<sup>29</sup> Although the POSS-norbornene has much higher ROMP activity than cyclooctadiene, sufficiently long reaction times (24 h) were chosen to allow significant interchain cross-metathesis to occur to ultimately afford random copolymers. The evidence for the random microstructures comes from <sup>1</sup>H NMR studies of the final copolymers; the copolymer with 53 wt % POSS in C<sub>2</sub>D<sub>2</sub>Cl<sub>4</sub> at 100 °C does not show any characteristic olefinic peaks from homopolymer of POSS-norbornene (Figure 4). Therefore, no significant amount of POSS-norbornene block segments is present in the copolymers.

**DSC.** The DSC data of PBD-POSS were collected and are shown in Figure 5. The lowest trace is a polybutadiene control. Each successive trace moving upward in the graph is increasing POSS wt %. Two clear transitions can be observed on all the curves in this graph. A glass transition temperature is shown around -95 °C, corresponding to  $T_g$  of 1,4-polybutadiene. A slight increase of  $T_g$  is observed in all of the PBD-POSS samples. The second peak around -10 °C comes from the melting transition of *trans*-1,4-polybutadiene. Be-

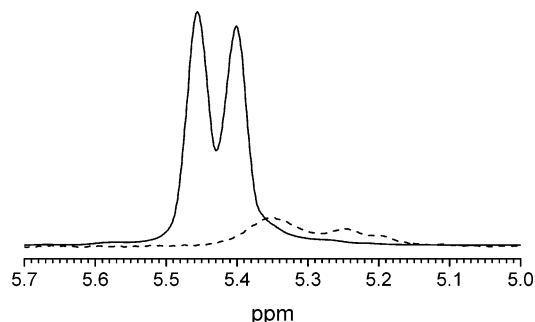


Figure 4. Olefinic region <sup>1</sup>H NMR spectra of poly(butadiene-POSS-53 wt %) copolymer (entry 6, Table 1, solid line) and poly(POSS-norbornene) (dashed line) at 100 °C in C<sub>2</sub>D<sub>2</sub>Cl<sub>4</sub>.

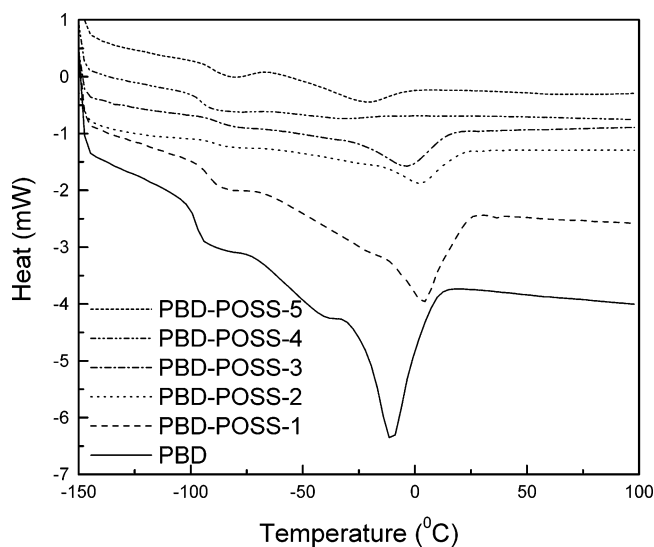
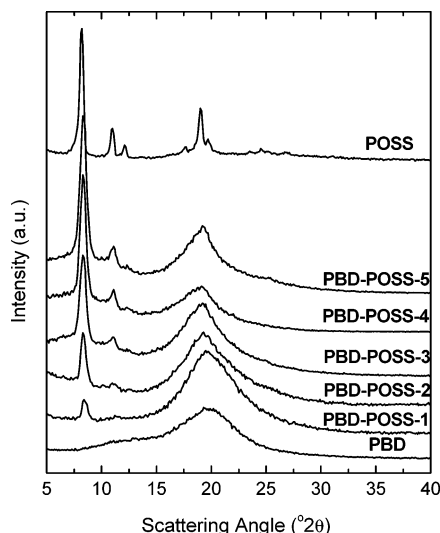


Figure 5. DSC traces of PBD and PBD-POSS copolymers.

cause of the lack of 1,2-units and relatively high trans content in PBD, a regular packing and crystallization of the chains becomes possible. With increasing POSS content in copolymers, the melting temperatures decrease from 5 to -20 °C from PBD-POSS-1 to PBD-POSS-5. This observation can be explained by the existence of POSS units in the copolymers, which disrupt the crystallization of PBD. A similar behavior was observed in PE- and PP-POSS copolymers, though at a much higher temperature range.<sup>30</sup> No significant transition is noticed from room temperature up to 400 °C, where the copolymers begin to degrade.

**WAXD.** Wide-angle X-ray diffraction, which provides information about crystalline structure, was used to examine these PBD-POSS samples for POSS aggregation and precise information on the crystalline lattice. Shown in Figure 6 are the diffraction profiles of PBD-POSS-1 to PBD-POSS-5. For comparison, traces of PBD and POSS are also drawn, respectively. The pure



**Figure 6.** WAXD of PBD-POSS. The sharp diffraction peaks at  $8.3^\circ$  (10.6 Å) and  $11.1^\circ$  (7.96 Å) indicate crystalline aggregation of POSS nanoparticles in PBD-POSS random copolymers.

PBD shows a broad peak at  $2\theta$ 's of  $19.5^\circ$  (4.55 Å), corresponding to an amorphous halo. The pure POSS shows strong reflections at  $2\theta$ 's of  $8.2^\circ$  (10.8 Å),  $11.0^\circ$  (8.03 Å),  $12.1^\circ$  (7.31 Å), and  $19.0^\circ$  (4.66 Å). These reflections are associated with the hexagonal crystalline structure of POSS from 101, 110, 012, and 300/113/330 diffraction planes with a hexagonal unit cell of  $a = 16.06$  Å and  $c = 17.14$  Å.<sup>40</sup> It is clear that the copolymers show features that are characteristic of the structures of the two separate components. For PBD-POSS-1, the sample with the lowest POSS content in this series, the WAXD is dominated by the PBD amorphous halo. However, an additional peak at  $8.3^\circ$  (10.6 Å) also appears. The next sample PBD-POSS-2 exhibits a third peak at  $11.1^\circ$  (7.96 Å). These peaks clearly correspond to the POSS reflections. As the POSS content increases, the reflections from the POSS component increase in intensity compared with the halo from PBD. At the highest POSS content, 53 wt % (10.8 mol %), the sample shows only a weak PBD amorphous halo and strong 101, 110 diffractions from POSS, leading to the conclusion that more and more POSS particles aggregate together to form a crystalline raftlike structure with increasing POSS concentration. The strong diffraction from POSS 300/113/330 diffraction planes observed at  $19^\circ$  is a broad peak overlapping with the halo from PBD due to close peak positions. In contrast to the sharp diffraction in POSS, the broadening at  $19^\circ$  is attributed to the anisotropic shape of the crystals.<sup>38</sup> In a constrained crystal lattice, the diffraction planes associated with the two long dimensions (length and width in a lamellar structure) show sharp diffraction, while diffractions associated with the one short dimension (thickness) show the broadest peaks.

**TEM.** Although the WAXD data indicate anisotropic crystalline aggregation of POSS nanoparticles in PBD-POSS random copolymers, this does not unambiguously prove the nanoscale morphology formed by POSS particles. As a result, transmission electron microscopy studies were carried out. The contrast in a TEM micrograph originates from diffraction and mass thickness contrast between dissimilar domains. POSS, due to its silicon content, has higher mass contrast than PBD chains which are comprised solely of carbon and hydrogen. In addition, the crystalline POSS domains as

observed by WAXD diffract electrons more effectively than amorphous PBD. Both of these effects render POSS darker in TEM imaging without the need to resort to a staining agent. Shown in Figure 7 are two natural contrast TEM micrographs of PBD-POSS random copolymers with 12 and 43 wt % POSS incorporation. In Figure 7A, POSS aggregates are directly observed as short randomly oriented lamellae with the lateral dimensions of approximately 50 nm. The thickness of the lamellae is found to be approximately 3–5 nm and corresponds to roughly twice the diameter of a POSS nanoparticle. The morphology observed here is comparable to that of fully exfoliated nylon-6/clay nanocomposites.<sup>43</sup> A notable feature of this sample is that this particular morphology was formed within 1 min, the time required for solvent evaporation. Increasing the incorporation ratio of POSS to 43 wt % results in continuous lamellae with lateral lengths on the order of microns (Figure 7C). The irregular lamellar spacing observed in the image is possibly a combination of both POSS lamella twisting and the random nature of the copolymers. The morphology bears similarity to the lamellar morphology formed by precise diblock copolymers. Interestingly, our experimental morphological results agree well with the computational result from Glotzer et al. on oligomeric tethered nanoparticles.<sup>44</sup> They predicted a similar nanostructure formation (Figure 3a,b in ref 44) using a system of oligomers tethered to specific locations on nanoparticles. The difference is that the simulation was carried out in a solvent, and the nanostructure was based on thermodynamically driven immiscibility of tethers and nanoparticles. The favorable particle-particle interaction to form the crystalline packing of POSS was not considered.

**SAXS.** The lamellar morphology formed via controlled self-assembly of POSS particles is further supported by the data of small-angle X-ray scattering (Figure 8), where broad maxima are observed. The peak positions correspond to the spacing  $d$  between lamellae. The value can be simply calculated using the equation  $d = 2\pi/q$ , where  $q = 4\pi/\lambda \sin(\theta/2)$  is the scattering vector. For example, the average distance between POSS layers is  $\sim 12$  nm in the PBD-POSS-4 sample. The lack of higher order reflections is a result of the random nature of the copolymers. The shift of broad maxima indicates that the spacing changes on the basis of the POSS concentrations. In a higher POSS concentration sample, such as PBD-POSS-5, the interlamellar distance is much smaller due to the relatively low PBD content between layers.

## Conclusions

A series of random copolymers of PBD and POSS bearing a polymerizable norbornene group were designed and successfully synthesized using ROMP copolymerization. The POSS loading in copolymers varies from 0 to 53 wt %, and molecular weights are in the range 67–88 kg/mol. The morphology of the copolymers has been characterized by WAXD, TEM, and SAXS. The results from WAXD show that the PBD-POSS copolymers have diffraction features of both POSS and PBD. In all the copolymers, POSS maintains the same crystalline structures or hexagonal packing with  $2\theta$ 's of  $8.3^\circ$  (10.6 Å) and  $11.1^\circ$  (7.96 Å) associated with (101) and (110) diffraction planes. TEM results indicate that the copolymers assemble into small, randomly oriented lamellae with lateral dimensions of approximately 50

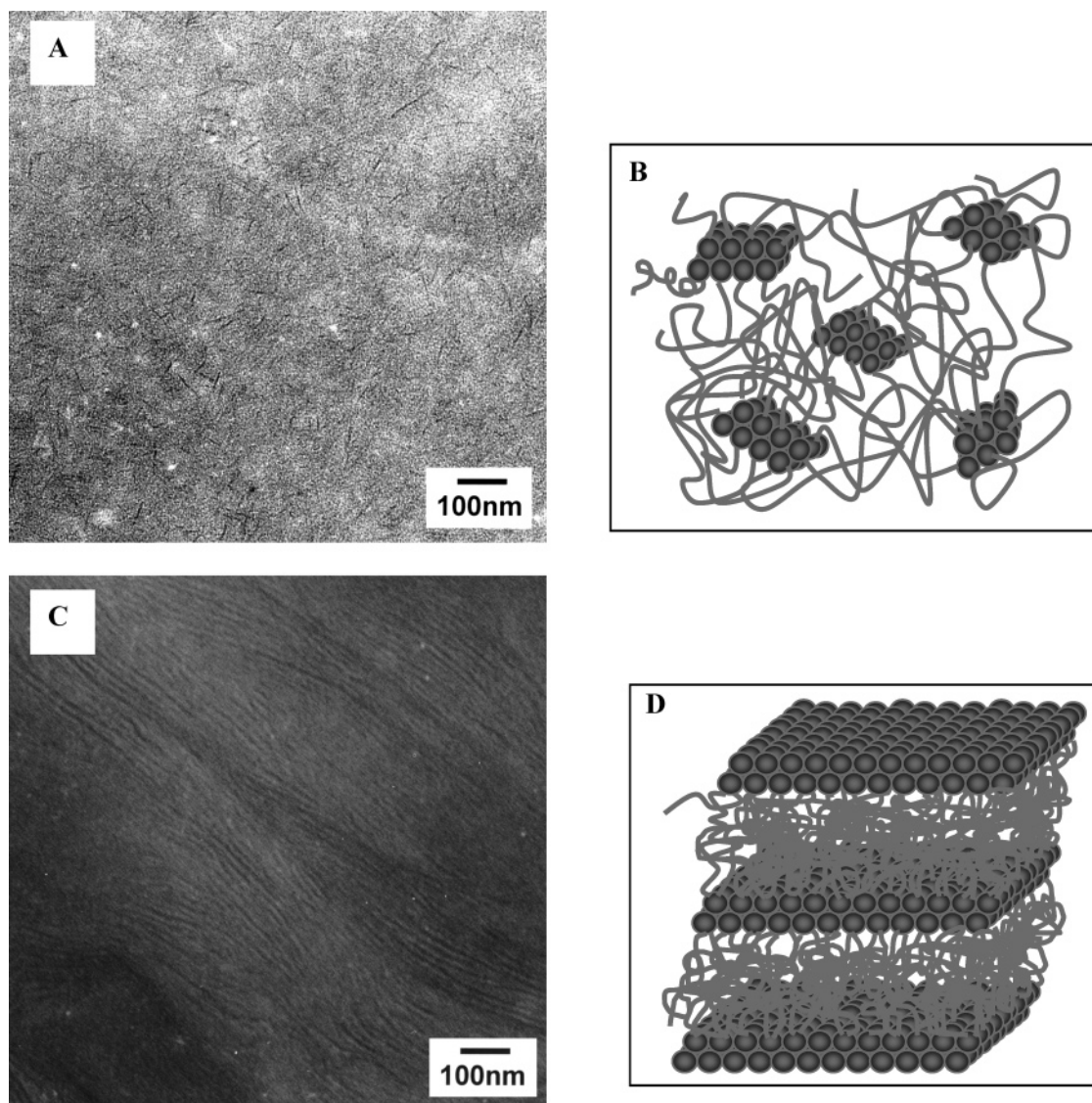


**Figure 7.** (A) TEM of PBD-POSS-1. The copolymers of low POSS concentration aggregate into short randomly oriented lamellae with lateral dimensions of approximately 50 nm. (B) Schematic drawing of PBD-POSS assembly at low POSS concentration. (C) TEM of PBD-POSS-4. The copolymers of high POSS concentration form continuous lamellar morphology with lateral length on the order of microns. (D) Schematic drawing of PBD-POSS assembly at high POSS concentration.

nm and thickness of 3–5 nm at low POSS concentration. These nanostructures extend to longer, continuous lamellar morphology with increasing POSS concentration. The spacing between lamellae can be changed by the relative ratio between POSS and PBD as shown by SAXS. The periodical spacing varies from 16 nm with 23 wt % POSS to 9.5 nm with 53 wt % POSS. All of these results clearly show the formation of self-assembled layered nanostructure of POSS aggregates. This design, based on associative interaction between POSS and limited crystal growth imposed by covalent attachment to a polymer backbone, may open the door to the design of ordered polymer materials at nanometer length scales that are well beyond the length scales of the primary sequences.

A second aspect of note is the design strategy. It is important to point out the difference between PBD-POSS nanocomposites and polymer clay nanocomposites in terms of their overall preparation, despite the similar morphologies observed under certain conditions. Polymer clay nanocomposites are one of the first successful demonstrations to emerge from the rapidly expanding field of nanoscale science.<sup>43,45,46</sup> They have shown sub-

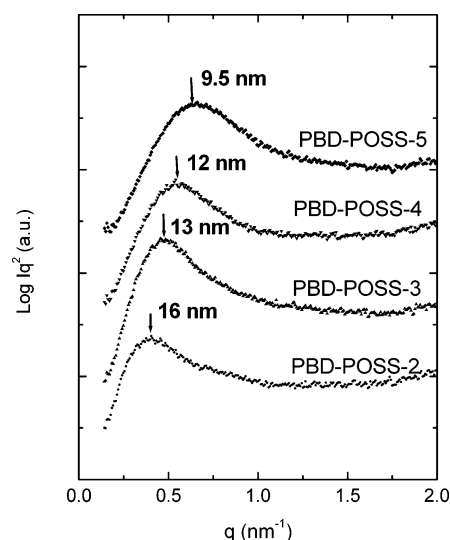


**Figure 8.** SAXS of PBD-POSS. The lamellar morphology formed via self-assembly of POSS particles is further supported by the data of small-angle X-ray scattering. The peak positions correspond to the spacing between lamellae.

stantial improvements in tensile strength and heat distortion temperature achieved at relatively low loadings of inorganic layered clays within a host polymer matrix. The attempt to disperse clay layers in a polymer matrix always encounters the problem of unfavorable interactions between the hydrophilic surface of clays and hydrophobic polymers. This results in an incomplete dispersal or limited exfoliation of clays. As a result, true polymer clay nanocomposites are successful only in a limited set of selected systems despite the fact that numerous attempts have been extended to incorporate clay filler in a broad range of polymeric materials. Generally speaking, the approach to obtain polymer clay nanocomposites involves a top-down strategy with a goal of separating macroscopic mineral clays into nanometer-sized individual layers. In contrast, the approach pursued in this work to build inorganic layered nanostructure using suitable self-assembly building blocks is a bottom-up approach. By switching the synthetic approach from top-down to bottom-up, the unfavorable interactions between the organic and inorganic components have been changed into a favorable factor. This approach can easily lead to a "homogeneous" organic-inorganic composite with nanometer thick inorganic layered filler uniformly distributed throughout the polymer matrix. Several of the novel properties documented in polymer/clay systems associated with the anisotropic shape of inorganic fillers are expected to be observed in assembled POSS systems.

The controlled aggregation of POSS spheres from single spherical particle to the ordered lamellar structures will offer a new opportunity for further understanding and better design of composite materials. Last, but not least, this controlled self-assembly process is also noteworthy considering the random nature of the copolymers and broad molecular weight distribution (polydispersity index  $\sim 2$ ). Other assembly methods, specifically surfactant and block copolymer approaches, require the use of well-defined molecules or polymers with low polydispersities. This work demonstrates that it is possible to obtain ordered nanostructure from a random copolymer system.

**Acknowledgment.** Financial support was provided by the University of Massachusetts, a NSF CAREER Award to E.B.C. (DMR-0239475), the NSF sponsored Materials Research Science and Engineering Center (MRSEC) at UMass (DMR-0213695), and the Army Research Laboratory Polymer Materials Center of Excellence (DAAD19-01-2-0002 P00005). L.Z. also thanks the Society of Plastic Engineers, Polymer Modifiers & Additives Division, for a partial scholarship.

## References and Notes

- Whitesides, G. M.; Mathias, J. P.; Seto, C. T. *Science* **1991**, *254*, 1312.
- Ikkala, O.; ten Brinke, G. *Science* **2002**, *295*, 2407.
- Hartgerink, J. D.; Beniash, E.; Stupp, S. I. *Science* **2001**, *294*, 1684.
- Matsen, M. W.; Bates, F. S. *Macromolecules* **1996**, *29*, 1091.
- Muthukumar, M.; Ober, C. K.; Thomas, E. L. *Science* **1997**, *277*, 1225.
- Aksay, I. A.; Trau, M.; Manne, S.; Honma, I.; Yao, N.; Zhou, L.; Fenter, P.; Eisenberger, P. M.; Gruner, S. M. *Science* **1996**, *273*, 892.
- Yang, H.; Kuperman, A.; Coombs, N.; MamicheAfara, S.; Ozin, G. A. *Nature (London)* **1996**, *379*, 703.
- Lu, Y. F.; Ganguli, R.; Drewien, C. A.; Anderson, M. T.; Brinker, C. J.; Gong, W. L.; Guo, Y. X.; Soyez, H.; Dunn, B.; Huang, M. H.; Zink, J. I. *Nature (London)* **1997**, *389*, 364.
- Lichtenhan, J. D. In *Polymeric Materials Encyclopedia*; Salamone, J. C., Ed.; CRC Press: Boca Raton, FL, 1996; p 7768.
- Choi, J.; Harcup, J.; Yee, A. F.; Zhu, Q.; Laine, R. M. *J. Am. Chem. Soc.* **2001**, *123*, 11420.
- Tamaki, R.; Tanaka, Y.; Asuncion, M. Z.; Choi, J.; Laine, R. M. *J. Am. Chem. Soc.* **2001**, *123*, 12416.
- Cassagneau, T.; Caruso, F. *J. Am. Chem. Soc.* **2002**, *124*, 8172.
- Tamaki, R.; Choi, J.; Laine, R. M. *Chem. Mater.* **2003**, *15*, 793.
- Lichtenhan, J. D.; Otonari, Y. A.; Carr, M. J. *Macromolecules* **1995**, *28*, 8435.
- Lichtenhan, J. D.; Vu, N. Q.; Carter, J. A.; Gilman, J. W.; Feher, F. J. *Macromolecules* **1993**, *26*, 2141.
- Haddad, T. S.; Lichtenhan, J. D. *Macromolecules* **1996**, *29*, 7302.
- Tsuchida, A.; Bolln, C.; Sernetz, F. G.; Frey, H.; Mulhaupt, R. *Macromolecules* **1997**, *30*, 2818.
- Lee, A.; Lichtenhan, J. D. *Macromolecules* **1998**, *31*, 4970.
- Romo-Urbe, A.; Mather, P. T.; Haddad, T. S.; Lichtenhan, J. D. *J. Polym. Sci., Part B: Polym. Phys.* **1998**, *36*, 1857.
- Schwab, J. J.; Lichtenhan, J. D. *Appl. Organomet. Chem.* **1998**, *12*, 707.
- Lee, A.; Lichtenhan, J. D. *J. Appl. Polym. Sci.* **1999**, *73*, 1993.
- Mather, P. T.; Jeon, H. G.; Romo-Urbe, A.; Haddad, T. S.; Lichtenhan, J. D. *Macromolecules* **1999**, *32*, 1194.
- Shockey, E. G.; Bolf, A. G.; Jones, P. F.; Schwab, J. J.; Chaffee, K. P.; Haddad, T. S.; Lichtenhan, J. D. *Appl. Organomet. Chem.* **1999**, *13*, 311.
- Fu, B. X.; Zhang, W. H.; Hsiao, B. S.; Rafailovich, M.; Sokolov, J.; Johansson, G.; Sauer, B. B.; Phillips, S.; Balnski, R. *High Perform. Polym.* **2000**, *12*, 565.
- Pyun, J.; Matyjaszewski, K. *Macromolecules* **2000**, *33*, 217.
- Costa, R. O. R.; Vasconcelos, W. L.; Tamaki, R.; Laine, R. M. *Macromolecules* **2001**, *34*, 5398.
- Fu, B. X.; Hsiao, B. S.; Pagola, S.; Stephens, P.; White, H.; Rafailovich, M.; Sokolov, J.; Mather, P. T.; Jeon, H. G.; Phillips, S.; Lichtenhan, J.; Schwab, J. *Polymer* **2001**, *42*, 599.
- Li, G. Z.; Wang, L.; Toghiani, H.; Daulton, T. L.; Koyama, K.; Pittman, C. U., Jr. *Macromolecules* **2001**, *34*, 8686.
- Zheng, L.; Farris, R. J.; Coughlin, E. B. *J. Polym. Sci., Part A: Polym. Chem.* **2001**, *39*, 2920.
- Zheng, L.; Farris, R. J.; Coughlin, E. B. *Macromolecules* **2001**, *34*, 8034.
- Li, G.; Wang, L.; Ni, H.; Pittman, C. U., Jr. *J. Inorg. Organomet. Polym.* **2002**, *11*, 123.
- Pittman, C. U., Jr.; Li, G.-Z.; Ni, H. *Macromol. Symp.* **2003**, *196*, 301.
- Leu, C.-M.; Chang, Y.-T.; Wei, K.-H. *Macromolecules* **2003**, *36*, 9122.
- Barry, A. J.; Daudt, W. H.; Domicone, J. J.; Gilkey, J. W. *J. Am. Chem. Soc.* **1955**, *77*, 4248.
- Larsson, K. *Ark. Kemi* **1960**, *16*, 203.
- Larsson, K. *Ark. Kemi* **1960**, *16*, 209.
- Larsson, K. *Ark. Kemi* **1960**, *16*, 215.
- Zheng, L.; Waddon, A. J.; Farris, R. J.; Coughlin, E. B. *Macromolecules* **2002**, *35*, 2375.
- Auf der Heyde, T. P. E.; Burgi, H.-B.; Burgi, H.; Tornroos, K. W. *Chimia* **1991**, *45*, 38.
- Waddon, A. J.; Coughlin, E. B. *Chem. Mater.* **2003**, *15*, 4555.
- Waddon, A. J.; Zheng, L.; Farris, R. J.; Coughlin, E. B. *Nano Lett.* **2002**, *2*, 1149.
- Schwab, P.; Grubbs, R. H.; Ziller, J. W. *J. Am. Chem. Soc.* **1996**, *118*, 100.
- Kojima, Y.; Usuki, A.; Kawasumi, M.; Okada, A.; Kurauchi, T.; Kamigaito, O. *J. Polym. Sci., Part A: Polym. Chem.* **1993**, *31*, 983.
- Zhang, Z. L.; Horsch, M. A.; Lamm, M. H.; Glotzer, S. C. *Nano Lett.* **2003**, *3*, 1341.
- Giannelis, E. P. *Adv. Mater.* **1996**, *8*, 29.
- Pinnavaia, T. J.; Beal, G. W., Eds. *Polymer Clay Nanocomposites*; John Wiley & Sons: New York, 2001.